J. Phase Equilib. Diffus. (2024) 45:639–652
https://doi.org/10.1007/s11669-024-01119-6

ORIGINAL RESEARCH ARTICLE

Phase Relations of the Sm–Ni–Al Ternary System at 800 °C in the 30–100 at.% Al Region

S. Delsante[1,2] · N. Parodi[1] · R. Novakovic[2] · G. Borzone[2]

Submitted: 29 December 2023 / in revised form: 25 March 2024 / Accepted: 6 May 2024 / Published online: 28 May 2024

Abstract The Sm–Ni–Al phase relationships at 800 °C have been investigated by using several well–focused experimental techniques such as X–Ray Powder Diffraction (XRPD), Light Optical Microscopy (LOM) and Scanning Electron Microscopy (SEM) coupled with Energy Dispersive Microprobe Analysis (EPMA). The isothermal section of the Sm–Ni–Al system at 800 °C was constructed according to the present experimental results. More than 50 alloys have been synthesized and characterized in the 30–100 at.% Al region. At 800 °C, 9 intermetallic phases have been confirmed, characterized and their relationships have been established. In the Al-rich corner, the presence of two ternary invariant reactions have been postulated whilst along the 16.67 at.% Sm isopleth, the presence of two structurally related extended solid solutions have been observed. The determined phase equilibria at 800 °C are discussed and compared with the isothermal section at 500 °C already reported in literature.

Keywords aluminum alloys · crystal structure · energy dispersive spectrometry (EDS) · experimental phase equilibria · isothermal section · ternary phase diagram · x-ray analysis

1 Introduction and Literature Review

The R–Ni and R–Ni–Al alloys are candidate for wide range of applications in various fields due to their comprehensive technological properties.[1,2]

Constitutional properties should be foremost among those to be studied to obtain a complete characterization of a metal system and thus of the phases existing therein. Knowledge of various aspects such as crystal structure, composition, thermodynamic properties, formation mechanism, and resulting microstructures is a prerequisite for a better understanding of the bonding mechanism and for the analysis of how a material can be prepared and used for certain purposes and under certain conditions.

A systematic study of the constitutional properties of alloys formed by rare earths elements (R) with aluminum and nickel has been underway in our laboratory for several years. Both, thermochemical approaches, such the determination of $\Delta_f H^0$ of selected binary and ternary phase,[3–6] and systematic research devoted to the study of phase relations and crystal chemistry[7–15] are being carried out.

1.1 Binary Boundary Systems

Structural (Pearson symbol, prototype and lattice parameters), compositional and temperature transformation data of the relevant phases of the binary subsystems are

This invited article is part of a special tribute issue of the *Journal of Phase Equilibria and Diffusion* dedicated to the memory of Thaddeus B. "Ted" Massalski. The issue was organized by David E. Laughlin, Carnegie Mellon University; John H. Perepezko, University of Wisconsin–Madison; Wei Xiong, University of Pittsburgh; and *JPED* Editor-in-Chief Ursula Kattner, National Institute of Standards and Technology (NIST).

✉ S. Delsante
simona.delsante@unige.it

[1] Department of Chemistry and Industrial Chemistry, Genoa University & INSTM Consortium, UdR di Genova, Via Dodecaneso 31, 16146 Genoa, Italy

[2] Institute of Condensed Matter Chemistry and Technologies for Energy, National Research Council of Italy (ICMATE-CNR), Via De Marini 6, 16149 Genoa, Italy

Table 1 Selected relevant phases of the binary Sm − Al, Ni − Al and Sm − Ni boundary systems: literature data on crystal structure and temperature transformation (see table footnote)

Phase/T (°C)	at.% Al	Pearson symbol-Prototype	Lattice parameters (Å)			References & notes
			a	*b*	*c*	
Al T_M = 660.45	100	*cF*4 − Cu	4.0433(2)	…	…	[16, 17]
$SmAl_3$ T_P = 1130	75	*hP*8 − Ni_3Sn	6.388(1)	…	4.607(1)	[11]
$NiAl_3$ T_P = 856	75	*oP*16 − Fe_3C	6.613(3)	7.367(6)	4.811(1)	[18]
$SmAl_2$ T_M = 1480	66.7	*cF*24 − $MgCu_2$	7.943(1)	…	…	[3]
Ni_2Al_3 T_P = 1138	60	*hP*5 − Ni_2Al_3	4.028(6)	…	4.891(5)	[19] (58.5 ÷ 64.3 at.%Al) At 60 at.% Ni [18]
NiAl T_M = 1639	50	*cP*2 − CsCl	2.8872	…	…	58.5 ÷ 28.8 at.% Al [19] at 50 at.% Ni [18]
Phase/ T (°C)	at.% Ni	Pearson symbol -Prototype	Lattice Parameters (Å)			
			a	*b*	*c*	
$SmNi_5$ T_M = 1433	83.3	*hP*6 − $CaCu_5$	4.9203(9)	…	3.9662(1)	[20]

T_M = melting temperature referred to elements or to congruent melting phases; T_P = peritectic decomposition.

summarized in Table 1. In the following few more information will be provided.

1.1.1 Al–Ni

The Al − Ni phase diagram has been thoroughly investigated and accordingly established by several studies (experimental investigations, assessment and thermodynamic optimization).[16,18,21–24] This system shows five intermediate phases: $NiAl_3$, Ni_2Al_3, NiAl, Ni_5Al_3 and Ni_3Al; only $NiAl_3$ is a "line compound", while the others present a certain solubility range. Solid Ni dissolves at 1371 °C (the Ni − rich eutectic temperature) a maximum of 21.2 at.% Al, while the solid solubility of Ni in Al is very limited.

*1.1.2 **Sm − Al***

The Sm − Al phase diagram[11,16,25] has the following intermediate phases: Sm_3Al_{11}, $SmAl_3$, $SmAl_2$, SmAl and Sm_2Al. It should be noted that the $SmAl_2$ phase forms congruently at quite high temperature (1480 °C) and shows a high negative enthalpy of formation (− 55.0 kJ/mol at[3]). The solid solubility of Sm in Al is very limited whereas only the formation of the solid solution in the γ-Sm has been established.

*1.1.3 **Sm − Ni***

The Sm − Ni system has been thoroughly experimentally investigated[26] and subsequently in the Sm–rich side two new phases Sm_7Ni_3 and Sm_3Ni_2 have been determined.[27] In addition, there are other eight intermediate phases (Sm_2Ni_{17}, $SmNi_5$, Sm_5Ni_{19}, Sm_2Ni_7, $SmNi_3$, $SmNi_2$, SmNi and Sm_3Ni) and the most recent assessment of the phase diagram is reported in.[28] Only the $SmNi_5$ phase is relevant for the present investigation (see Table 1).

1.2 Ternary Sm–Ni–Al System

The alloying behaviour of the three elements (Sm, Ni and Al) is characterized by the formation of many ternary phases, as summarized in Table 2.

A partial isothermal section of the Sm–Ni–Al system at 500 °C (40–100 at.% Al region) was determined by[12]; at this temperature, six ternary compounds were found and characterized ($Sm_4Ni_6Al_{23}$, $SmNiAl_4$, $SmNiAl_3$, $SmNi_2Al_3$, $SmNiAl_2$ and SmNiAl). A small homogeneity range

Table 2 Sm–Ni–Al system: literature data on crystal structures and lattice parameters of the ternary phases and solid solution of binary phases

#	Phase	Stoichiometric composition (at.%)			Pearson symbol –prototype and method	Lattice Parameters (Å)	References/ Comments
		Sm	Ni	Al			
1	$Sm_3Ni_5Al_{19}$	11.1	18.5	70.4	*oS*108–$Gd_3Ni_5Al_{19}$	a = 4.0992(1)	[13], at 800 °C
					Powder diffraction	b = 16.0304(3)	
						c = 27.1050(5)	
2	$Sm_4Ni_6Al_{23}$	12.12	18.18	69.7	*mS*66 – $Y_4Ni_6Al_{23}$	a = 15.939(3)	[10]
					Single crystal	b = 4.0967(6)	
						c = 18.320(3)	
						β = 113.09(2)°	
3	$SmNiAl_4$	16.67	16.67	66.66	*oS*24–$YNiAl_4$	a = 4.0948(6)	[9]
					Single crystal	b = 15.582(3)	
						c = 6.610(1)	
4	$SmNiAl_3$	20.0	20.0	60.0	*oP*20–$YNiAl_3$	a = 8.197(4)	[12], at 500 °C
					Powder diffraction	b = 4.087(2)	
						c = 10.713(1)	
5	$Sm_3Ni_7Al_{14}$	12.5	29.2	58.3	*hP*72–$Gd_3Ni_7Al_{14}$	a = 18.047(5)	[29]
					Powder diffraction	c = 4.059(1)	
6	$SmNi_2Al_3$	16.67	33.33	50.0	*hP*18 – YNi_2Al_3	a = 9.141(3)	[12], at 500 °C,
	(*)				Powder diffraction	c = 4.039(1)	
7	$SmNiAl_2$	25.0	25.0	50.0	o*S*16–$CuMgAl_2$	a = 4.025(5)	[30]
					Powder diffraction	b = 10.46(2)	[12], at 500 °C
						c = 6.868(6)	
						a = 4.058(3)	
						b = 10.519(7)	
						c = 6.903(5)	
8	SmNiAl	33.33	33.33	33.33	*hP*9–ZrNiAl	a = 6.982(9)	[31]
					Powder diffraction	c = 4.008(2)	[32]
						a = 6.986(1)	
						c = 4.010(1)	
9	$Sm_3Ni_6Al_2$	27.3	54.5	18.2	*cI*44–$Ce_3Ni_6Al_2$	a = 7.7994(2)	[33]
					Powder diffraction		
	$SmAl_{2-x}Ni_x$	33.3	(x/3)%	66.7-(x/3)%	c*F*24 – Cu_2Mg	a = 7.937(1)	[12], at 500 °C
					Powder diffraction	(x = 0.075)	0 < x < 0.21
						a = 7.881(5)	
						(x = 0.21)	
	$SmAl_{3-x}Ni_x$	25.0	(x/4)%	75.0-(x/4)%	*hP*8–Ni_3Sn	a = 6.389(2)	[12], at 500 °C
					Powder diffraction	c = 4.607(1)	0 < x < 0.06
						(x = 0)	
10	$SmNi_{5-x}Al_x$	16.7	66.6-(x/6)%	(x/6)%	*hP*6–$CaCu_5$	a = 5.043(3)	[34]
					Powder diffraction	c = 4.072(1)	0 < x < 1.5
						(x = 1.5)	

(*) see text (sub-section 3.5) for the description of the range of composition of the phase described as "$SmNi_{2+x}Al_{3-x}$".

for $SmNiAl_4$ and $SmNi_2Al_3$ ternary phases was found; for the $SmNiAl_4$ the Al content varyied from ~ 67 to 65 at.% and that of Ni from ~ 17 to 19 at.%, whereas for the $SmNi_2Al_3$ the composition ranges from (~49 at.% Al, ~ 34.3 at.% Ni, 16.67 at.% Sm) to (~52.5 at.% Al, ~ 30.8 at.% Ni, 16.67 at.% Sm) was observed. The binary phases $SmAl_2$ and $SmAl_3$ dissolve up to 7 and 1.5 at.% Ni at constant Sm content, whereas NiAl dissolves up to 1 at.% Sm.

The effect of the rare earth addition on the phase equilibria and microstructure of Ni–Al alloys at high Al–content (> 70 at.%) was subsequently studied at 800 °C by,[15] confirming the presence of the ternary phase $Sm_3Ni_5Al_{19}$ at higher temperature as already reported in.[13] Furthermore, Matselko et al.[29] discovered the existence of another ternary compound $Sm_3Ni_7Al_{14}$ in samples annealed at 800 °C and then quenched.

Considering the summarized literature data, the determination of the phase equilibria at 800 °C has been performed in the 30–100 at.% Al composition range synthesizing and completely characterizing more than 50 alloys. In the present work, besides the clarification of various two and three-phases fields, some differences were observed with respect to the phase equilibria already determined at 500 °C.[12] In addition, the relationships of the phases in the Al–rich region were modified compared to our previous work[15] and the Sm alloying behaviour towards Ni and Al will be discussed.

2 Experimental Details

Pieces of pure metals (Al, WAV AG ''Kryal'' 99.999; Ni, JM Alfa Aesar 99.99 and Sm, JM Alfa Aesar 99.9 minimum mass% purity) were polished, weighed in the proper amount, and then melted in alumina crucibles by induction melting under flowing argon. The samples were re-melted several times under continuous shaking to attain proper homogenization and, generally, no weight loss was observed after melting. After the synthesis, samples were inserted in small alumina crucibles placed in flame-sealed quartz ampoules in an Ar atmosphere and then kept at 800 °C for different times depending on the alloy composition (from 15 to 90 days). After the annealing, an ice-water quenching was carried out.

Pieces of the samples were resin-mounted and smoothed firstly by grinding with SiC abrasive papers up to 1200 mesh and then by lapping with special cloths coated with diamond abrasive spray down to 1 μm size. A Light Optical Microscope (LOM) was employed to check the status of the polishing procedure and have an overview of the microstructure (i.e. number of phases and their distribution). Generally, no etching was necessary.

Next, a thorough investigation of each sample was performed using an Electron Scanning Microscope (Zeiss-EVO 40) with a Back-Scattered Electron detector (BSE) to exploit the compositional contrast between the different phases. Quantitative Electron Probe Microanalysis (EPMA) data were collected at 20 kV with an x-ray Spectroscopy (EDS) detector (Oxford INCA X-ACT). Certified pure elements were used as reference standards, and for calibration, cobalt was adopted; the software package Inca Energy (Oxford Instruments, Analytical Ltd., Bucks, U.K.) was employed to process x-Ray Spectra. EDS analyses were performed for each phase in various portions of the sample using both area and spot analysis, and the final composition was averaged from the quantitative results; generally, an error within 0.5 at.% was assigned for each element.

x-Ray Diffraction analysis on powdered samples (XRPD) was performed for both phase identification and measurement of lattice parameters. A *Philips X'Pert* MPD machine (Philips, Almeno, The Netherlands) equipped with a copper target, excited to 40 kV and 30 mA, and a solid-state detector was used in the 2ϑ angular range 10°–100°. The XRPD patterns were indexed by PowderCell[35] and lattice parameters were calculated by a least-squares method.[36]

3 Results and Discussion

The experimental results for selected samples concerning the overall EDS composition, the phase detected by both SEM/EDS and XRPD analysis (including the composition of the phases and the measured lattice parameters, when available) and details about annealing time are reported in Table 3. For the samples not included in Table 3, see the "*Supporting information*" section (Table S). In addition, average values of the lattice parameters determined for binary and ternary phases for all samples, are summarized in Table 4. The different areas of the isothermal section are described and discussed in the following sub-sections.

3.1 Revised Al–Rich Corner

The Al–rich part of the phase diagram (from ∼ 64 to 100 at.% Al) is characterized by the presence of three ternary phases ($Sm_4Ni_6Al_{23}$, $Sm_3Ni_5Al_{19}$ and $SmNiAl_4$) which are involved in several equilibria including the $SmAl_3$, $SmAl_2$, $NiAl_3$ and Ni_2Al_3 binary phases. During this work, 25 alloys have been synthesized and fully characterized in this portion of the phase diagram. The measured lattice parameters of the ternary and binary phases are in very good agreement with literature data (see the values summarized in Tables 1 and 2 in comparison with the experimental data obtained during this work). The phases compositions are also in good agreement with the stoichiometric ones, taking account of the error associated with the EDS measurement (see Table 3). Considering the small difference in the composition of the ternary phases $Sm_3Ni_5Al_{19}$ and $Sm_4Ni_6Al_{23}$, the results obtained by XRPD analysis were essential to distinguish them.

The phase equilibria determined are slightly different in comparison with our previous work[15]; furthermore, the

Table 3 SEM/EDS experimental results of selected Sm –Ni –Al alloys annealed at 800 °C and then water quenched

#	Alloy EDS composition (at.%)			Observed phases	EDS Phase composition (at.%)			Lattice parameters (Å)				Remarks
	Sm	Ni	Al		Sm	Ni	Al	a	b	c	β	
1	2.0	7.0	91.0	$Sm_3Ni_5Al_{19}$	12.0	18.7	69.3	4.0978(5)	16.022(4)	27.120(6)	…	Figure 1a 15d
				$NiAl_3$	…	24.0	76.0	…	…	…	…	
				Liquid	1.3	2.7	96.0	…	…	…	…	
2	2.0	8.5	89.5	$Sm_3Ni_5Al_{19}$	11.8	18.6	69.6	4.0980(5)	16.020(3)	27.105(6)	…	Figure 1b 15d
				$NiAl_3$	…	24.0	76.0	6.6146(4)	7.3702(5)	4.8150(3)	…	
				Liquid	1.4	2.8	95.8	…	…	…	…	
3	11.0	5.5	83.5	$Sm_4Ni_6Al_{23}$	12.6	18.6	68.8	15.938(1)	4.0969(1)	18.320(5)	113.1(2)	Figure 2a 15d
				$SmAl_3$	25.5	…	74.5	6.3841(5)	…	4.5999(5)	…	
				Liquid	2.5	2.0	95.5	…	…	…	…	
4	16.2	3.1	80.7	$Sm_4Ni_6Al_{23}$	12.7	18.5	68.8	15.939(8)	4.0971(2)	18.320(2)	113.1(4)	Figure 2b 30d
				$SmAl_3$	25.1	…	74.9	6.3845(6)	…	4.5996(5)	…	
				Liquid	2.0	1.5	96.5	…	…	…	…	
5	5.8	21.7	72.5	$Sm_3Ni_5Al_{19}$	12.0	18.4	69.6	4.0984(2)	16.022(1)	27.089(2)	…	Figure 3a 30d
				$NiAl_3$	…	24.5	75.5	6.6145(4)	7.3706(2)	4.8152(3)	…	
				Ni_2Al_3	…	39.0	61.0	4.0531(7)	…	4.9052(3)	…	
6	1.0	29.5	69.5	$Sm_3Ni_5Al_{19}$	12.0	18.6	69.4	4.0979(3)	16.019(1)	27.143(2)	…	Figure 3b 30d
				$NiAl_3$	…	25.0	75.0	6.6142(3)	7.3701(3)	4.8151(2)	…	
				Ni_2Al_3	…	39.0	61.0	4.0530(2)	…	4.9049(4)	…	
7	21.0	10.0	69.0	$SmNiAl_4$	17.2	16.5	66.3	4.0949(2)	15.581(5)	6.6105(3)	…	Figure 4a 30d
				$SmAl_2$	33.8	…	66.2	7.9428(4)	…	…	…	
				$SmAl_3$	24.5	…	75.5	6.3854(5)	…	4.6002(3)	-	
8	17.5	14.0	68.5	$Sm_4Ni_6Al_{23}$	12.8	18.6	68.6	15.939(2)	4.0966(3)	18.320(8)	113.1(5)	Figure 5a 30d
				$SmNiAl_4$	17.5	17.0	65.5	4.0946(3)	15.582(3)	6.6095(2)	…	
				$SmAl_3$	26.0	…	74.0	…	…	…	…	
9	30.5	3.7	65.8	$SmNiAl_4$	17.5	16.5	66.0	4.0953(5)	15.584(1)	6.6108(6)	…	Figure 4b 30d
				$SmAl_2$	34.2	…	65.8	7.9430(1)	…	…	…	
				$SmAl_3$	26.0	…	74.0	…	…	…	…	
10	10.3	25.7	64.0	$Sm_4Ni_6Al_{23}$	12.6	18.5	68.9	…	…	…	…	Figure 5b 60d
				$SmNiAl_4$	17.4	16.5	66.1	4.0954(4)	15.589(2)	6.6098(7)	…	
				Ni_2Al_3	…	39.0	61.0	4.0593(7)	…	4.8960(6)	…	
11	12.0	25.0	63.0	$SmNiAl_4$	17.3	16.4	66.3	4.0973(8)	15.600(3)	6.6100(1)	…	30d
				NiAl	…	45.7	54.3	…	…	…	…	
12	22.2	15.6	62.2	$SmNiAl_4$	17.2	16.8	66.0	4.0963(6)	15.577(6)	6.6108(1)	…	Figure 6a 58d
				$SmNiAl_3$	59.4	20.0	20.6	…	…	…	…	
				$SmAl_2$	34.0	…	66.0	7.9365(3)	…	…	…	
13	17.0	21.5	61.5	$SmNiAl_4$	17.2	17.0	65.8	4.1041(3)	15.603(1)	6.6107(6)	…	75d

Table 3 continued

#	Alloy EDS composition (at.%)			Observed phases	EDS Phase composition (at.%)			Lattice parameters (Å)				Remarks
	Sm	Ni	Al		Sm	Ni	Al	a	b	c	β	
				$SmNiAl_3$	20.0	20.5	59.5	8.1875(6)	4.0912(3)	10.702(1)	…	
				$Sm_3Ni_7Al_{14}$	13.1	30.3	56.6	18.096(1)	…	4.0635(3)	…	
14	22.0	18.0	60.0	$SmNiAl_3$	20.8	20.2	59.0	8.1874(3)	4.0912(1)	10.703(3)	…	Figure 6b 60d
				$SmNi_2Al_3$	17.4	32.9	49.7	…	…	…	…	
				$SmAl_2$	34.0	…	66.0	7.9376(2)	…	…	…	
15	3.0	38.0	59.0	$SmNiAl_4$	17.2	16.8	66.0	4.0958(5)	15.586(2)	6.6106(6)	…	60d
				Ni_2Al_3	…	43.3	56.7	4.0354(5)	…	4.902(2)	…	
				NiAl	…	45.9	54.1	…	…	…	…	
16	11.5	30.0	58.5	$SmNiAl_4$	17.4	16.8	65.8	…	…	…	…	Figure 8a 60d
				$Sm_3Ni_7Al_{14}$	13.0	29.0	58.0	18.056(1)	…	4.0592(3)	…	
				NiAl	…	49.0	51.0	2.8779(8)	…	…	…	
17	31.0	11.0	58.0	$SmNiAl_2$	25.9	24.9	49.2	4.0583(4)	10.521(1)	6.9032(5)	…	60d
				$SmAl_2$ (ss 2.5 at.% Ni)	33.9	2.4	63.7	7.932(1)	…	…	…	
18	7.5	36.0	56.5	$SmNiAl_4$	17.0	17.1	65.9	4.0942(7)	15.581(2)	6.609(1)	…	Figure 7 30d
				NiAl	…	48.0	52.0	2.8711(8)	…	…	…	
19	10.0	35.5	54.5	$SmNi_2Al_3$	17.0	33.9	49.1	…	…	…	…	Figure 8b 30d
				$Sm_3Ni_7Al_{14}$	13.0	30.8	56.2	18.052(1)	…	4.0587(2)	…	
				NiAl	…	49.0	51.0	2.879(1)	…	…	…	
20	15.5	30.5	54.0	$SmNiAl_3$	20.4	20.7	58.9	8.186(1)	4.0911(5)	10.701(1)	…	60d
				$SmNi_2Al_3$	17.0	33.0	50.0	9.139(2)	…	4.040(2)	…	
				$Sm_3Ni_7Al_{14}$	13.0	30.2	56.8	18.051(2)	…	4.0587(6)	…	
21	23.5	23.5	53.0	$SmNiAl_2$	25.1	25.4	49.5	4.0587(5)	10.525(2)	6.9053(9)	…	30d
				$SmNi_2Al_3$	17.1	33.5	49.4	…	…	…	…	
				$SmAl_2$ (ss 2.5 at% Ni)	33.5	2.6	63.9	7.9294(3)	…	…	…	
22	28.0	20.0	52.0	$SmNiAl_2$	25.5	25.3	49.2	4.0581(5)	10.522(2)	6.9036(9)	…	30d
				SmNiAl	32.0	33.2	34.8	…	…	…	…	
				$SmAl_2$ (ss 9 at.% Ni)	34.2	9.0	56.8	7.8516(1)	…	…	…	
23	15.7	46.7	37.6	$SmNi_{2+x}Al_{3-x}$ (x ~ 0.85)	17.0	47.0	36.0	8.8511(3)	…	4.1295(2)	…	Figure 9a 30d
				NiAl	…	51.0	49.0	2.8880(4)	…	…	…	
24	14.8	50.8	34.4	$SmNi_{5-x}Al_x$ (x ~ 1.9)	17.0	51.0	32.0	5.0870(5)	…	4.0871(6)	…	Figure 9b 30d
				NiAl	…	51.0	49.0	…	…	…	…	
25	21.0	54.0	25.0	$Sm_3Ni_6Al_2$	27.1	54.6	18.3	7.7990(4)	…	…	…	30d
				$SmNi_{5-x}Al_x$ (x ~ 1.6)	16.8	55.8	27.4	…	…	…	…	

L: liquid phase. d: days of annealing. ss: solid solution. The experimental results of all characterized samples are included in the Table S ("*Supporting Information*").

Table 4 Summary of the XRPD experimental results obtained on binary and ternary phases (average values of the lattice parameters)

Phase	Crystal structure	Lattice parameters			
		a [Å]	*b* [Å]	*c* [Å]	*β*
$Sm_3Ni_5Al_{19}$	*oS*108–$Gd_3Ni_5Al_{19}$	4.0982(3)	16.021(1)	27.116(2)	…
$Sm_4Ni_6Al_{23}$	*mS*66–$Y_4Ni_6Al_{23}$	15.939(3)	4.0968(2)	18.320(1)	113.1(3)
$SmNiAl_4$	*oS*24–$YNiAl_4$	4.0949(3)	15.583(3)	6.6103(4)	…
$SmNiAl_3$	*oP*20–$YNiAl_3$	8.1889(4)	4.0912(4)	10.702(1)	…
$Sm_3Ni_7Al_{14}$	*hP*72–$Gd_3Ni_7Al_{14}$	18.070(3)	…	4.0590(3)	…
$SmNiAl_2$	*oS*16–$CuMgAl_2$	4.0584(5)	10.523(2)	6.9033(7)	…
$SmNi_2Al_3$	*hP*18–YNi_2Al_3	9.139(2)	…	4.040(2)	…
$Sm_3Ni_6Al_2$	*cI*44–$Ce_3Ni_6Al_2$	7.7990(4)	…	…	…
$SmAl_3$	*hP*8–$SnNi_3$	6.3837(5)	…	4.6000(5)	…
$SmAl_2$	*cF*24–$MgCu_2$	7.9393(3)	…	…	…
$SmAl_2$ (ss, ~ 2.5 at.% Ni)	*cF*24–$MgCu_2$	7.9307(2)	…	…	…
$SmAl_2$ (ss, ~ 9 at.% Ni)	*cF*24–$MgCu_2$	7.8516(1)	…	…	…
$NiAl_3$	*oP*16 – Fe_3C	6.6144(4)	7.3704(3)	4.8152(3)	…
Ni_2Al_3 (~57 at.% Al)	*hP*5 – Ni_2Al_3	4.0354(5)	…	4.902(2)	…
Ni_2Al_3 (~61 at.% Al)	*hP*5 – Ni_2Al_3	4.0530(1)	…	4.9051(4)	…
NiAl (~49 at.% Al)	*cP*2 – CsCl	2.8883(4)	…	…	…
NiAl (~52 at.% Al)	*cP*2 – CsCl	2.8711(8)	…	…	…
$SmNi_{5-x}Al_x$ (x = 1.9)	*hP*6 – $CaCu_5$	5.0870(5)	…	4.0868(6)	…
$SmNi_{2+x}Al_{3-x}$ (x = 0.85)	*hP*18 – YNi_2Al_3	8.8511(3)	…	4.1295(2)	…

ss: solid solution, see text.

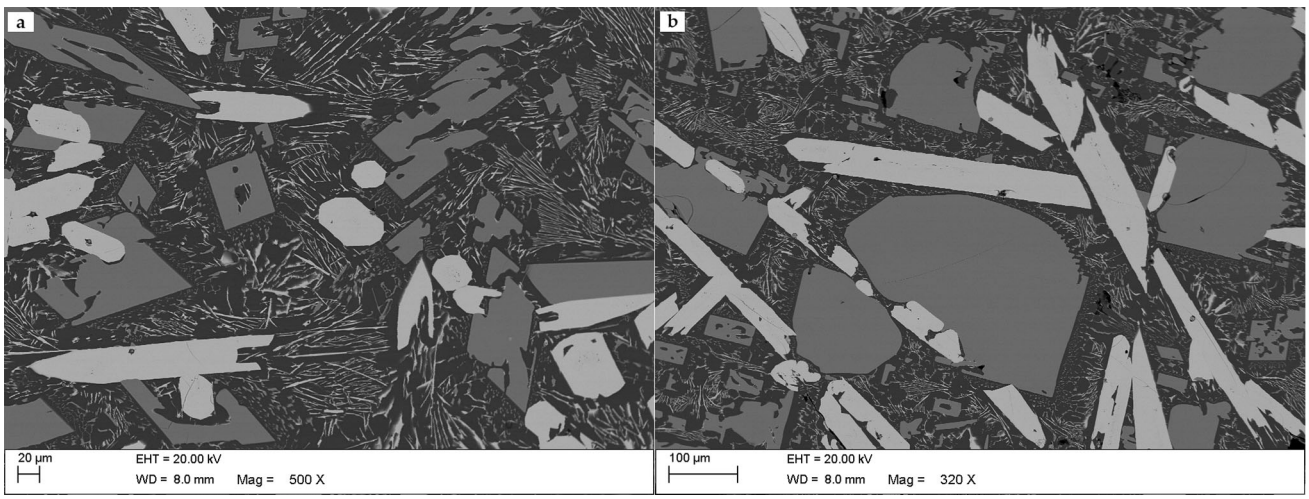

Fig. 1 (a, b) SEM image (BSE mode), samples #1 (1a) and #2 (1b) in Table 3. $NiAl_3$ (grey phase), $Sm_3Ni_5Al_{19}$ (white phase), Al (black phase) in the eutectic-like mixture (liquid phase). Some cracks and holes are visible in 1b (black portions)

previously postulated solubility of Ni in the $SmAl_3$ phase has not been confirmed. The relationships observed involving the relevant phases are the following: $Sm_4Ni_6Al_{23} + SmAl_3 + L$; $Sm_3Ni_5Al_{19} + NiAl_3 + L$; $SmNiAl_4 + SmAl_3 + SmAl_2$; $Sm_4Ni_6Al_{23} + SmNiAl_4 + SmAl_3$; $Sm_3Ni_5Al_{19} + NiAl_3 + Ni_2Al_3$; $Sm_4Ni_6Al_{23} + SmNiAl_4 + Ni_2Al_3$. In addition, two ternary fields ($Sm_3Ni_5Al_{19} + Sm_4Ni_6Al_{23} + L$ and $Sm_3Ni_5Al_{19} + Sm_4Ni_6Al_{23} + Ni_2Al_3$) have been postulated considering boundary conditions. It should be noted that the relationship between the ternary phases $Sm_3Ni_5Al_{19}$ and $Sm_4Ni_6Al_{23}$ with the liquid phase was reported in.[14] The composition of the Ni_2Al_3 involved in the listed two- and three-phase fields is ~ 61 at.% Al.

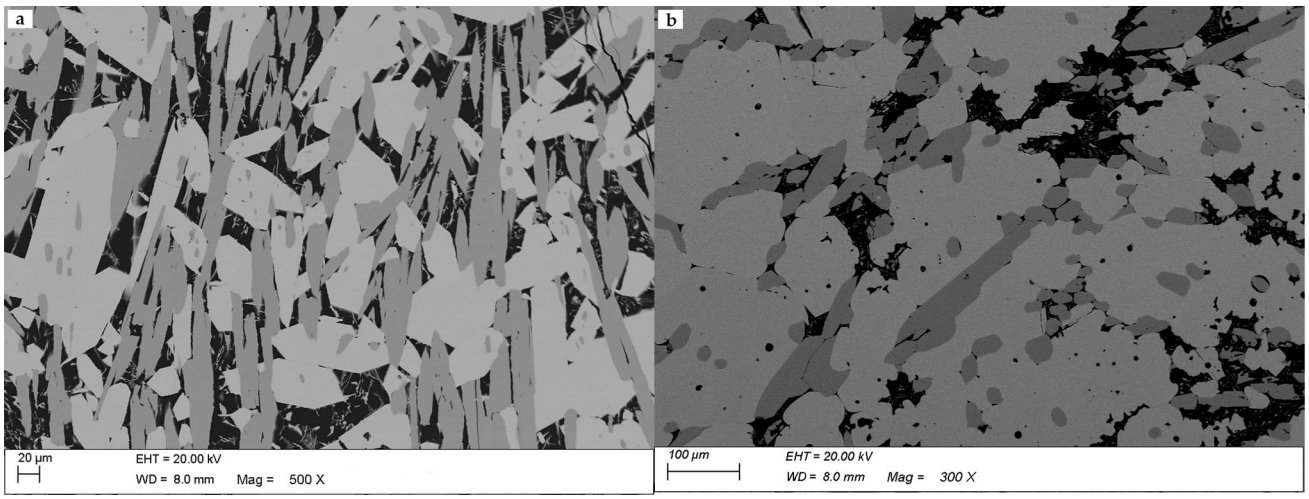

Fig. 2 (a, b) SEM image (BSE mode), samples #3 (2a) and #4 (2b) in Table 3. $SmAl_3$ (white phase), $Sm_4Ni_6Al_{23}$ (light-grey phase), Al (black phase) in the eutectic-like mixture (liquid phase)

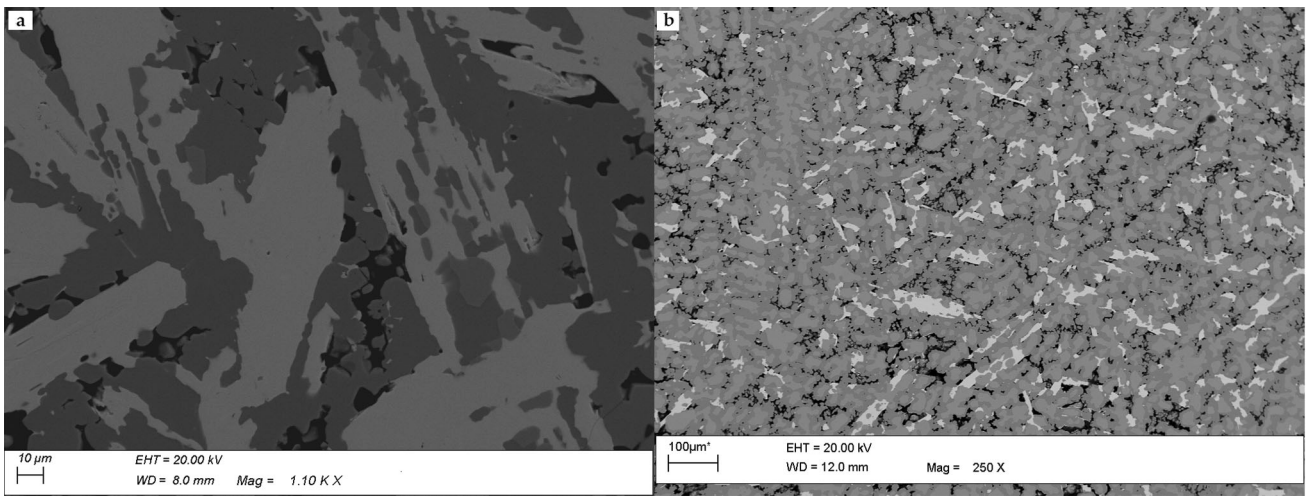

Fig. 3 (a, b) SEM image (BSE mode), samples #5 (3a) and #6 (3b) in Table 3. $NiAl_3$ (dark grey phase), Ni_2Al_3 (light grey phase), $Sm_3Ni_5Al_{19}$ (bright/white phase). Cracks and holes are visible (black portions)

Selected images acquired by SEM (BSE mode) showing the microstructure appearance of the alloys belonging to these ternary fields of the ternary isothermal section are shown in Figs. 1, 2, 3, 4 and 5.

Figure 1(a, b) (samples #1 and #2, respectively) and 2(a, b) (samples #3 and #4, respectively) highlight the peculiarity of the alloys annealed in the presence of the liquid phase; it is possible to notice the big crystals of two phases, $NiAl_3$ and $Sm_3Ni_5Al_{19}$ (Fig. 1a, b) and $SmAl_3$ with $Sm_4Ni_6Al_{23}$ (Fig. 2a, b), are surrounded by a fine mixture of the same phases in equilibrium with pure Al. Figure 3(a, b) (samples #5 and #6, respectively) shows the equilibria of the two binary phases $NiAl_3$ and Ni_2Al_3 with the $Sm_3Ni_5Al_{19}$; this result modifies the one previously reported equilibria[15] in which the three-phase equilibria in this portion of the diagram were: $Sm_4Ni_6Al_{23} + Sm_3Ni_5Al_{19} + Ni_2Al_3$ and $Sm_4Ni_6Al_{23} + Sm_3Ni_5Al_{19} + NiAl_3$. The microstructure of two selected samples showing the relationship among the binary phases $SmAl_3$ and $SmAl_2$ with $SmNiAl_4$, is shown in Fig. 4(a, b) (samples #7 and #9, respectively). In Fig. 5(a) (sample #8) big crystals of $SmNiAl_4$ are surrounded by a mixture of $Sm_4Ni_6Al_{23}$ and $SmAl_3$, whereas in Fig. 5(b) (sample #10) an "eutectic-like" mixture of $SmNiAl_4$ and Ni_2Al_3 is prevalent in comparison to a small amount of $Sm_4Ni_6Al_{23}$ (bottom right corner of the image).

3.2 $SmAl_{2-x}Ni_x$ Relationships at 800 °C

The binary $SmAl_2$ phase shows a solubility toward Ni of up to ~ 9 at.% by the substitution of Al; this behaviour could be unexpected considering the limited solubility of Ni in

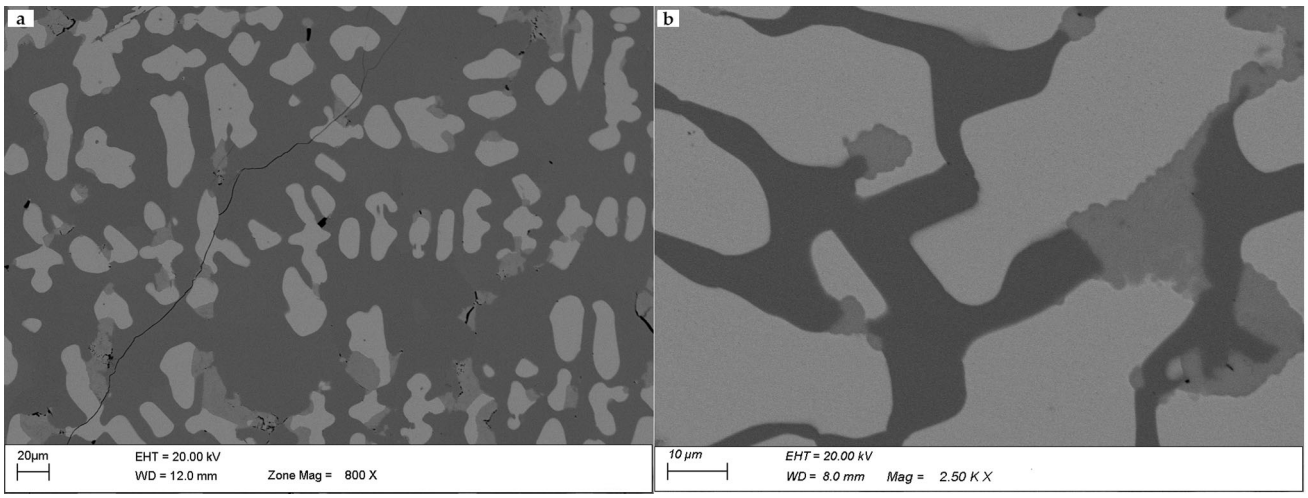

Fig. 4 (a, b) SEM image (BSE mode), samples #7 (4a) and #9 (4b) in Table 3. $SmAl_2$ (white phase), $SmAl_3$ (light grey phase), $SmNiAl_4$ (dark grey phase). Some cracks and holes are visible in 4a (black portions)

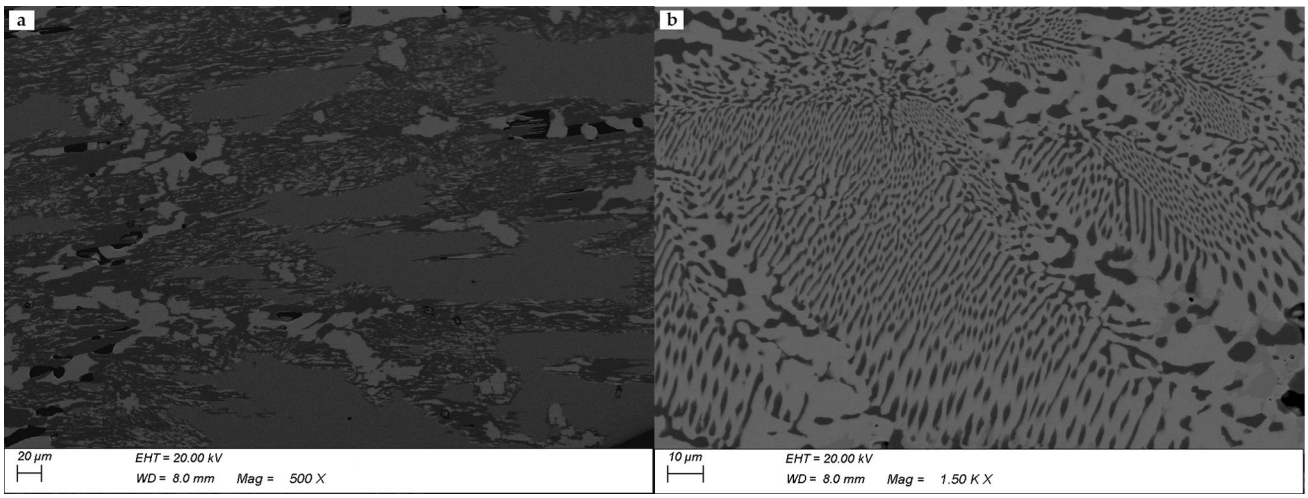

Fig. 5 (a, b) SEM image (BSE mode), samples #8 (5a) and #10 (5b) in Table 3. 5a: $SmAl_3$ (bright phase), $SmNiAl_4$ (grey phase), $Sm_4Ni_6Al_{23}$ (dark grey phase); 5b: Ni_2Al_3 (dark grey phase), $SmNiAl_4$ (light grey phase), $Sm_4Ni_6Al_{14}$ (grey phase, small amount). Some cracks and holes are visible in 5a (black portions)

Al[16]; however, we observed a solubility of Ni in $SmAl_2$ of up to ~ 7 at.% at 500 °C.[12] The $SmAl_2$ phase (both stoichiometric or containing Ni) is involved in several two- and three-phase regions; indeed, the following three-phase equilibria have been observed: $SmNiAl_4 + SmAl_3 + SmAl_2$ (already discussed), $SmNiAl_4 + SmNiAl_3 + SmAl_2$; $SmNiAl_3 + SmNi_2Al_3 + SmAl_2$; $SmNiAl_2 + SmNi_2Al_3 + SmAl_2$ (solid solution with ~ 2.5 at.% Ni); $SmNiAl_2 + SmNiAl + SmAl_2$ (solid solution with ~ 9 at.% Ni). As expected, a decrease in the lattice parameter "*a*" of the cubic $SmAl_2$ phase (*cF*24–$MgCu_2$) by increasing the Ni content has been observed and then quantified by XRPD analysis (see value reported in Table 4); in addition, a very good agreement with the "*a*" value calculated in this work for the $SmAl_2$ solid solution (with ~ 2.5 at.% Ni) and the value reported in[12] for the same composition, should be noted. As for the XRPD results on the ternary phases, a good agreement has been observed by comparing the literature data (see Table 2) with the experimental ones determined during this work (see Table 4). This evidence led us to conclude that the ternary phases involved in the discussed equilibria do not have a significant composition ranges of existence despite the slightly different values obtained by SEM/EDS analysis (see Table 3). In particular, the Al content for the $SmNi_2Al_3$ phase was never measured to be higher than 50 at.%.

The SEM/BSE microstructure of sample #12 shown in Fig. 6(a), illustrates the three-phase field "$SmAl_2 + SmNiAl_3 + SmNiAl_4$"; the bright phase $SmAl_2$, with

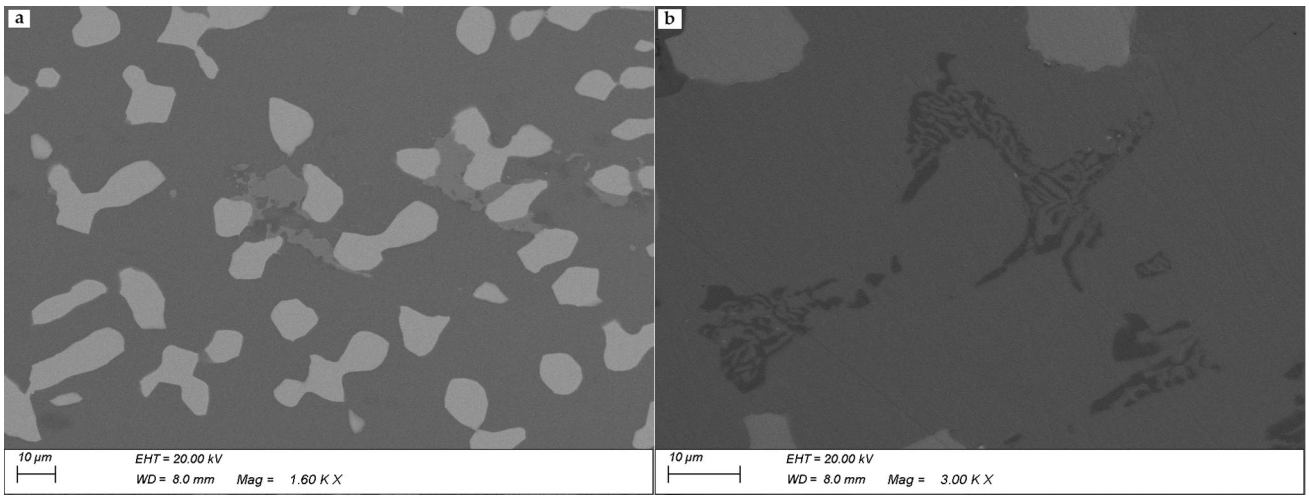

Fig. 6 (a, b) SEM image (BSE mode), samples #12 (6a) and #14 (6b) in Table 3. 6a: $SmAl_2$ (bright phase), $SmNiAl_3$ (light grey phase), $SmNiAl_4$ (grey phase); 6b: $SmAl_2$ (bright phase), $SmNiAl_3$ (grey phase), $SmNi_2Al_3$ (dark grey phase, small amount)

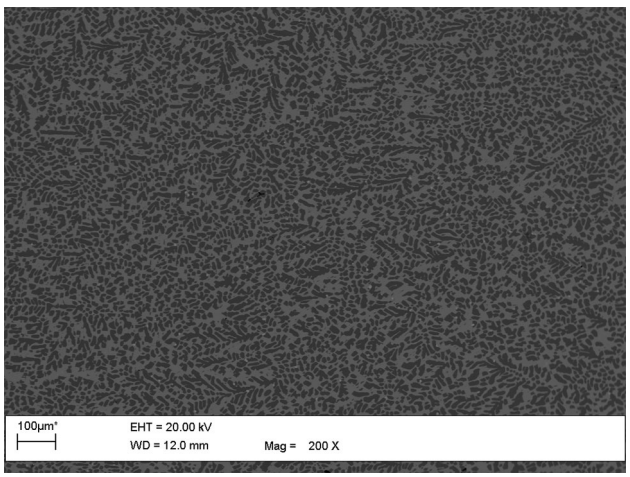

Fig. 7 SEM image (BSE mode), samples #18 in Table 3. NiAl (black phase), $SmNiAl_4$ (dark grey phase)

stoichiometric composition, is surrounded by the grey phase $SmNiAl_4$ and a small amount of $SmNiAl_3$. In Fig. 6(b) (sample #14) it is possible to observe the bright $SmAl_2$ phase in equilibrium with $SmNiAl_3$ (grey phase) and a small amount of $SmNi_2Al_3$ (dark grey phase). The phase relationships observed in this part of the isothermal section are fairly similar to those observed at 500 °C[12]; the main differences concern the extent of Ni solubility in the $SmAl_2$ phase (up to ~ 7 at.% Ni at 500 °C *vs.* ~ 9 at.% Ni at 800 °C) and the stoichiometric compositions of the $SmNiAl_4$ and $SmNi_2Al_3$ phases at 800 °C, unlike those observed at 500 °C.

3.3 Equilibria Involving Ni_2Al_3 and NiAl Phases

Both binary Ni_2Al_3 and NiAl phases have a homogeneity range of existence[19]; this feature plays a role in the established two- and three-phase equilibria at 800 °C. As for the Ni_2Al_3, the measured composition ranges from ~ 57 to ~ 61 at.% Al, whereas NiAl ranges from ~ 49 to ~ 54 at.% Al; both phases do not form a solid solution with Sm. In addition to the already discussed established relationships with $Sm_4Ni_6Al_{23}$ and $Sm_3Ni_5Al_{19}$ (see sub-section 3.1), both phases are involved in the two- and three-phase equilibria with $SmNiAl_4$; the three-phase field is formed by NiAl (~54 at.% Al) + Ni_2Al_3 (~57 at.% Al) + $SmNiAl_4$. As an example, Fig. 7, shows the microstructure of the two-phase sample #18 in which the NiAl black phase (with ~ 52 at.% Al) is mixed with the dark-grey phase $SmNiAl_4$. The calculated lattice parameters of the binary phases are in good agreement with the literature data[19] and confirm the measured EDS composition. The NiAl phase is also in equilibrium with the $Sm_3Ni_7Al_{14}$ phase, to be discussed in the next sub-section (3.4); this phase seems to have a wide field of primary crystallization.

3.4 $Sm_3Ni_7Al_{14}$ Relationships at 800 °C

Chronologically, this is the last ternary phase discovered and described in literature[29]; as reported therein and confirmed by our previous work,[12] this phase seems to be stable in samples annealed at 800 °C but not in those annealed at 500 °C. A common feature of the alloys belonging to this part of the isothermal section was the need of longer annealing (up to 90 days) to obtain samples in equilibrium. $Sm_3Ni_7Al_{14}$ exists in the following three-phase equilibria: $SmNiAl_4 + SmNiAl_3 + Sm_3Ni_7Al_{14}$; $SmNiAl_4 + Sm_3Ni_7Al_{14} + NiAl$; $Sm_3Ni_7Al_{14} + SmNi_2Al_3 + NiAl$ and $SmNiAl_3 + Sm_3Ni_7Al_{14} + SmNi_2Al_3$. The measured compositions of the ternary phases are in

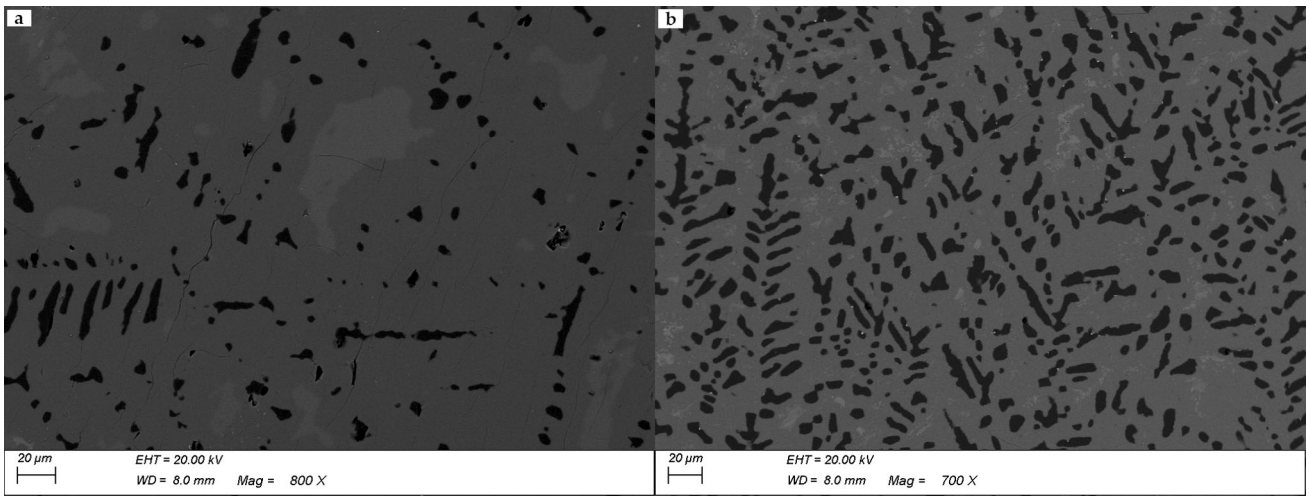

Fig. 8 (a, b) SEM image (BSE mode), samples #16 (8a) and #19 (8b) in Table 3. 8a: NiAl (black phase), $SmNiAl_4$ (grey phase), $Sm_3Ni_7Al_{14}$ (light grey phase); 8b: NiAl (black phase), $Sm_3Ni_7Al_{14}$ (grey phase), $SmNi_2Al_3$ (light grey phase, small amount)

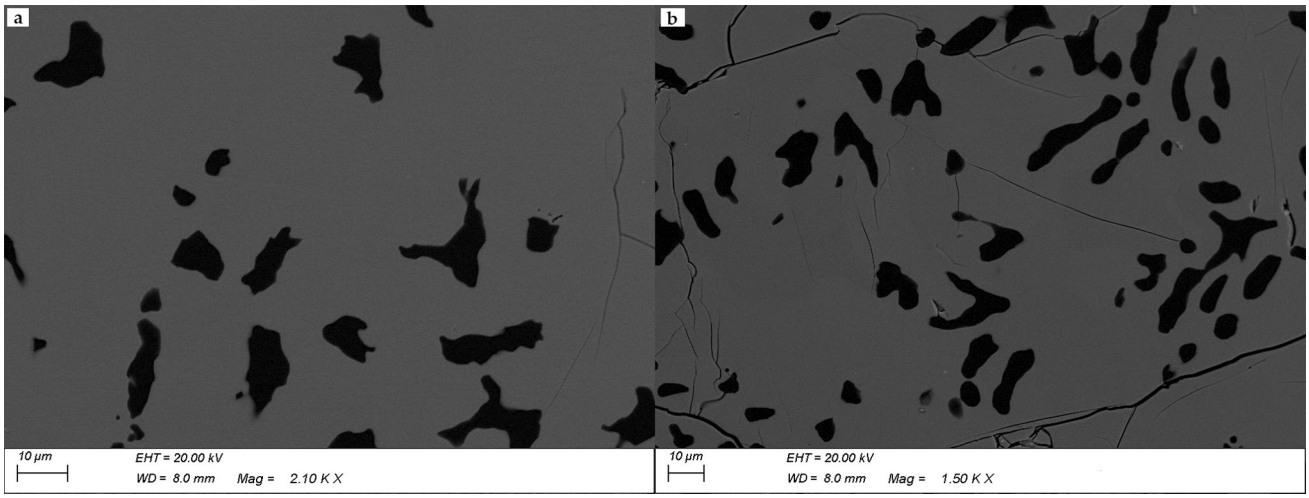

Fig. 9 (a, b) SEM image (BSE mode), samples #23 (9a) and #24 (9b) in Table 3. 9a: NiAl (black phase) and $SmNi_{2+x}Al_{3-x}$ (grey phase); 9b: NiAl (black phase) and $SmNi_{5-x}Al_x$ (grey phase). Cracks and holes are visible (black portions)

good agreement with the stoichiometric ones and the calculated lattice parameters obtained by XRPD analysis agree with the literature data (see the comparison of values listed in Tables 2 and 4). In this region of the isothermal section, the measured EDS composition of the NiAl phase was $\sim$ 51 at.% Al, with a negligible solubility towards Sm and a lattice parameter a = 2.878(1) Å.

Since the $Sm_3Ni_7Al_{14}$ phase is not stable at 500 °C, the equilibria in this part of the diagram are very different from those determined in the isothermal section at 500 °C[12]; indeed, at lower temperature, around the composition of this ternary phase, there is the three-phase field "NiAl + $SmNiAl_4$ + $Sm_4Ni_6Al_{23}$". The microstructure appearance in which the NiAl phase is in equilibrium with the two ternary phases $SmNiAl_4$ and $Sm_3Ni_7Al_{14}$ is shown in Fig. 8(a) (samples #16) whilst the Fig. 8(b) belongs to sample #19: the NiAl black phase is surrounded by the $Sm_3Ni_7Al_{14}$ (grey phase) and by a small amount of the light grey $SmNi_2Al_3$ phase.

3.5 $SmNi_{5-x}Al_x$ and $SmNi_{2+x}Al_{3-x}$ Relationships

Starting from the $SmNi_5$ phase ($hP6$–$CaCu_5$) a quite wide solid solution toward Al, at a constant content of 16.7 at.% Sm, is reported in literature. The higher determined content of Al was with x = 1.5.[34] Besides, a solid solution having an $hP18$–YNi_2Al_3 structure, was found; this can be described with the variable stoichiometry "$SmNi_{2+x}Al_{3-x}$" ($0 < x < 0.5$).[12,34] The unit cell parameters of the two type structures, $hP6$–$CaCu_5$ and $hP18$–YNi_2Al_3, are correlated by the following relationships: $a_{hP18} = a_{hP6}\sqrt{3}$ and $c_{hP18} = c_{hP6}$; the YNi_2Al_3 type structure was considered as a

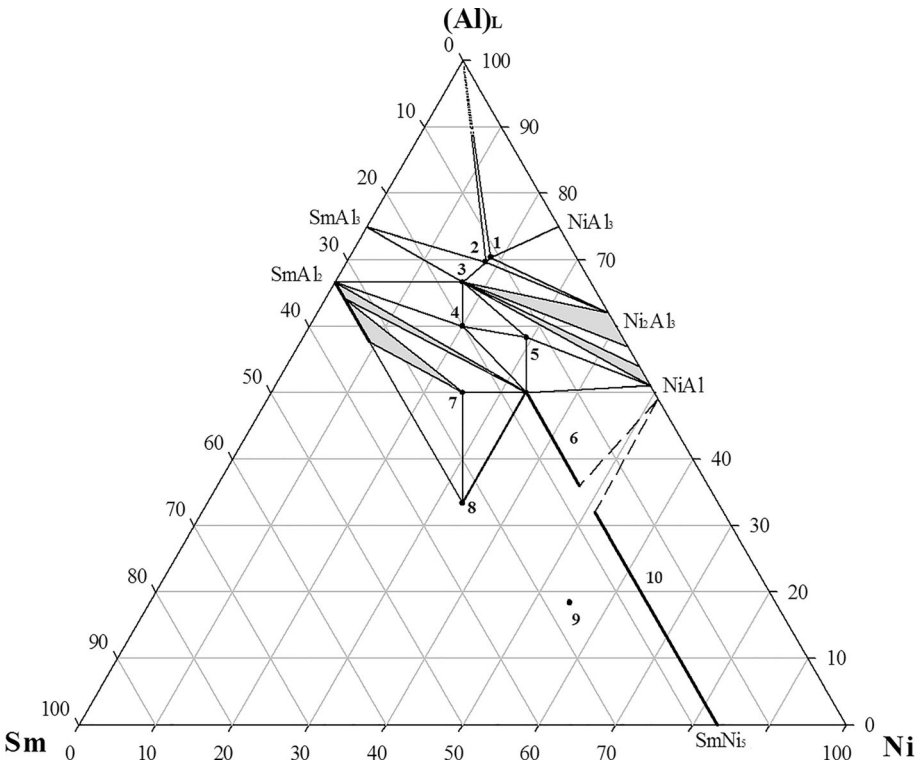

Fig. 10 Sm–Ni–Al system: isothermal section at 800 °C in the 30–100 at.% Al composition range. The observed ternary phases are reported: (1) $Sm_3Ni_5Al_{19}$; (2) $Sm_4Ni_6Al_{23}$; (3) $SmNiAl_4$; (4) $SmNiAl_3$; (5) $Sm_3Ni_7Al_{14}$; (6) $SmNi_{2+x}Al_{3-x}$; (7) $SmNiAl_2$; (8) SmNiAl; (9) $Sm_3Ni_6Al_2$; (10) $SmNi_{5-x}Al_x$. A dotted liquidus line has been sketched (see text for details). The two-phase fields having a certain homogeneity range have been coloured in light grey. The Sm corner has not been investigated

P6/mmm hexagonal superstructure of the $RNi_{5-x}Al_x$ phase (R = Rare Earth element with a $CaCu_5$ type[37]), which is located on the same R 16.67 at.% isopleth line.

During this work, several two-phase samples containing the NiAl phase (with an Al content ~ 49 at.%) together with $SmNi_{5-x}Al_x$ phase or $SmNi_{2+x}Al_{3-x}$ (see Table 3 and "*Supporting Information*", Table S) have been synthesized and characterized. The range of existence of both phases was extended: for the *hP*6 phase ($SmNi_{5-x}Al_x$) a x ~ 1.9 was measured (~ 32 at.% Al) whilst for the *hP*18 phase ($SmNi_{2+x}Al_{3-x}$) the determined x was ~ 0.85 (~ 36 at.% Al); therefore, the new observed ranges of existence of the two phases are: $0 < x <$ ~ 1.9 for the *hP*6 phase and $0 < x < 0.85$ for the *hP*18 one. The determined lattice parameters are summarized in Table 4.

For both samples, the microstructures are similar, as can be seen in Fig. 9(a) (sample #23) and 9b (sample #24): the black NiAl phase is surrounded by a matrix of the grey phase $SmNi_{2+x}Al_{3-x}$ or $SmNi_{5-x}Al_x$.

4 Conclusions and Future Perspectives

The aim of this study was to fill up the gap in the information about the phase equilibria in the Sm–Ni–Al system, occurring at 800 °C in the 30–100 at.% Al region; the obtained isothermal section is shown in Fig. 10 in which 18 three-phase equilibria have been observed.

Regarding the boundary systems Sm–Al and Ni–Al, only the $SmAl_2$ phase showed solubility towards the third element; in fact, a maximum content of ~ 9 at.% Ni was determined at the expense of the amount of Al; higher than that reported at 500 °C.[12] In addition, the range of the existence of the $SmNi_{5-x}Al_x$ (*hP*6-$CaCu_5$) solid solution has been deepened; the maximum detected Al content was ~ 32 at.% (x ~ 1.9, higher than x = 1.5 previously reported[34]). In addition, the rather wide existence interval of another solid solution that can be described as "$SmNi_{2+x}Al_{3-x}$", having the *hP*18–YNi_2Al_3 structure, was confirmed and extended up to an Al content of ~ 36 at.% (x ~ 0.85, higher than x = 0.5[34]). Nevertheless, it was not possible to define whether there is an "order-disorder" transition between them or a zone where both coexist, and which would therefore allow to trace the "$SmNi_{2+x}Al_{3-x}$ + $SmNi_{5-x}Al_x$ + NiAl" three-phase field.

The existence of all ternary phases reported in literature was confirmed as well as their stoichiometry; from this point of view, it was important to couple the SEM/EDS analysis with the XRPD investigation. As an example, the two most Al-rich ternary phases, $Sm_4Ni_6Al_{23}$ and $Sm_3Ni_5Al_{19}$, are very close in composition; therefore, XRPD analysis was essential to distinguish them without any uncertainty.

New results acquired during this work have partially modified the previously published isothermal section[15]: the solubility of Ni in the $SmAl_3$ phase has not been

confirmed and the three-phase field "$Sm_4Ni_6Al_{23}$ + $NiAl_3$ + Ni_2Al_3" was replaced by "$Sm_3Ni_5Al_{19}$ + $NiAl_3$ + Ni_2Al_3" whilst the three-phase equilibrium field "$Sm_4Ni_6Al_{23}$ + $Sm_3Ni_5Al_{19}$ + Ni_2Al_3" was drawn instead of "$Sm_4Ni_6Al_{23}$ + $Sm_3Ni_5Al_{19}$ + $NiAl_3$". The phase equilibria studied during this work at 800 °C and those previously studied at 500 °C[12] are significantly different, as the two phases $Sm_3Ni_5Al_{19}$ and $Sm_3Ni_7Al_{14}$ were not found in samples annealed at 500 °C.

The formation at 800 °C of the $R_3Ni_5Al_{19}$ and RNi_3Al_9 (R = rare earth metal) phases is typical for *heavy* rare earths (Gd–Lu and Y); both are not stable for La, Ce, Pr and Nd (*light* rare earths).[14] Our experimental evidence for the Sm–Ni–Al system of the presence of the former and not the latter confirmed a "*borderline*" behaviour of Sm when alloyed with Al and Ni.

The microstructures observed for compositions > 80 at.% Al suggests the possible presence of a ternary eutectic L ⇄ (Al) + $Sm_4Ni_6Al_{23}$ + $SmAl_3$ in the region close to the Sm–Al system and another invariant reaction in the region close to the Ni–Al system involving the 4 phases "L + (Al) + $Sm_3Ni_5Al_{19}$ + $NiAl_3$". Considering that the $Sm_3Ni_5Al_{19}$ phase is not stable at 500 °C, assuming invariant reactions in this narrow area of the phase diagram is daring at present and would require not only targeted thermal analysis experiments, but also computational support (i.e. with the CALPHAD technique).

Funding Open access funding provided by Università degli Studi di Genova within the CRUI-CARE Agreement.

Supplementary Information The online version contains supplementary material available at https://doi.org/10.1007/s11669-024-01119-6.

References

1. K.H.J. Buschow, in Hydrogen Absorption in Intermetallic Compounds Handbook on the Physics and Chemistry of Rare Earths. In: K. A. Jr Gschneidner, L. Eyring (Eds.), (North-Holland Physics Publishing: Amsterdam, 1984), pp. 1–111
2. V.K. Pecharsky, and K.A. Gschneidner Jr., Gschneidner, Some Common Misconceptions Concerning Magnetic Refrigerant Materials, *J. Appl. Phys.*, 2001, **90**, p 4614–4622.
3. G. Borzone, A. Cardinale, A. Saccone, and R. Ferro, Enthalpies of Formation of Solid Sm–Al Alloys, *J. Less-Comm. Met.*, 1995, **220**(1–2), p 122–125.
4. G. Borzone, N. Parodi, R. Raggio, and R. Ferro, Thermodynamic Investigation of Samarium–Nickel Alloys, *J. Alloys Compd.*, 2001, **317–318**, p 532–536.
5. G. Borzone, R. Raggio, S. Delsante, and R. Ferro, Chemical and Thermodynamic Properties of Several Al–Ni–R Systems, *Intermetallics*, 2003, **11**(11–12), p 1217–1222.
6. S. Delsante, R. Stifanese, and G. Borzone, Thermodynamic Stability of RNi_2 Laves Phases, *J. Chem. Thermodyn.*, 2013, **65**, p 73–77.
7. A. Saccone, G. Cacciamani, D. Macciò, G. Borzone, and R. Ferro, Contribution to the Study of the Alloys and Intermetallic Compounds of Aluminium with the Rare-Earth Metals, *Intermetallics*, 1988, **6**, p 201–215.
8. R. Raggio, G. Borzone, and R. Ferro, The Al–Rich Region in the Y-Ni–Al System: Microstructures and Phase Equilibria, *Intermetallics*, 2000, **8**(3), p 247–257.
9. M.L. Fornasini, R. Raggio, and G. Borzone, Crystal Structure of Samarium Nickel Tetraaluminide, $SmNiAl_4$, *Z. Kristallogr. NCS*, 2004, **219**, p 75–76.
10. M.L. Fornasini, R. Raggio, and G. Borzone, Crystal Structure of Samarium Nickel Aluminide, $Sm_4Ni_6Al_{23}$, *Z. Kristallogr. NCS*, 2004, **219**, p 77–78.
11. S. Delsante, R. Raggio, G. Borzone, and R. Ferro, Investigation of Al–rich Part of Sm–Al Binary System, *J. Phase Equilib. Diffus.*, 2007, **28**(3), p 240–242.
12. S. Delsante, R. Raggio, and G. Borzone, Phase Relations of the Sm–Ni–Al Ternary System at 500 °C in the 40–100 at.% Al Region, *Intermetallics*, 2008, **16**, p 1250–1257.
13. S. Delsante, K.W. Richter, H. Ipser, and G. Borzone, Synthesis and Structural Characterization of Ternary Compounds Belonging to the Series $RE_{2+m}Ni_{4+m}Al_{15+4m}$ (RE = Rare Earth Metal), *Z. Anorg. Allg. Chem.*, 2009, **635**, p 365–368.
14. S. Delsante, and G. Borzone, The Gd–Ni–Al System: Phases Formation and Isothermal Sections at 500 °C and 800 °C, *Intermetallics*, 2014, **45**, p 71–79.
15. S. Delsante, N. Parodi, and G. Borzone, Effect of the Rare-Earth Addition (R = Ce, Sm) on the Phase Equilibria and Microstructure of Ni–Al Alloys, *J. Phase Equilib. Diffus.*, 2014, **35**, p 421–428.
16. T.B. Massalski, H. Okamoto, P.R. Subramanian, L. Kacprzak (Eds.), (1990) Binary Alloys Phase Diagrams, Vols. 1–3, 2nd edition, Materials Park, OH, USA.
17. H.M. Otte, W.G. Montague, and D.O. Welch, x-Ray Diffractometer Determination of the Thermal Expansion Coefficient of Aluminium Near Room Temperature, *J. Appl. Phys.*, 1963, **34**, p 3149–3150.
18. P. Saltykov, L. Cornish and G. Cacciamani, Al–Ni (Aluminium-Nickel), MSIT Binary. Evaluation Program, in MSIT Workplace, Effenberg, G. (Ed.), MSI, Material Science International Services GmbH, Stuttgart; (2003) (Equi. Diagram, Review, 164).
19. P. Nash and C.H. Tung, in: *Phase Diagrams of Binary Nickel Alloys*, P. Nash, Ed., ASM International, Materials Park, OH, 1991, p 62−67.
20. K. Nouri, M. Jemmali, S. Walha, K. Zehani, A. Ben Salah, and L. Bessais, Structural, Atomic Hirschfeld Surface, magnetic and Magnetocaloric Properties of SmNi5 Compound, *J. Alloys Compd.*, 2016, **672**, p 440–448.
21. Y. Du, and N. Clavaguera, Thermodynamic Assessment of the Al–Ni System, *J. Alloys Compd.*, 1996, **237**, p 20–32.

22. I. Ansara, N. Dupin, H.-L. Lukas, and B. Sundman, Thermodynamic Assessment of the Al–Ni System, *J. Alloys Compd.*, 1997, **247**(1–2), p 20–30.
23. W. Huang, and Y.A. Chang, A Thermodynamic Analysis of the Ni–Al System, *Intermetallics*, 1998, **6**, p 487–498.
24. J.C. Schuster, Paper presented at COST535 meeting, Paris; March (2004).
25. K.H.J. Buschow, Rare Earth-Aluminium Intermetallic Compounds of the form RAl and R_3Al_2, *J. Less-Comm. Metals*, 1965, **8**, p 209–212.
26. Y.Y. Pan, and C.S. Cheng, A Phase Diagram of the Alloys of the Samarium-Nickel Binary System, *Acta Phys. Sinica*, 1983, **32**, p 92–95.
27. G. Borzone, Y. Yuan, S. Delsante, and N. Parodi, The Sm–Ni System: New Phases in the Sm–rich Region, *Monatsh. Chem.*, 2012, **143**, p 1299–1307.
28. H. Okamoto, Supplemental Literature Review of Binary Phase Diagrams: Al-Ni, B-Hf, Ca–Sc, Cr–Sc, Fe–Rh, Hf–Mn, La–Sb, Ni–Re, Ni–Sm, Ni–Zr, Sb–Tb and Ti–Zr, *J. Phase Equilib. Diffus.*, 2019, **40**, p 830–841.
29. O. Matselko, S.Y. Pukas, R.E. Gladyshevskii, and N. Chornenkaya, New Compounds in R–Ni–Al Systems, *Diffusion and Defect Data—Solid State Data*, *Pt. B: Solid State Phenomena*, 2011, **170**, p 397a.
30. G. Bruzzone, M. Ferretti, F. Merlo, and G. Olcese, Structural, Magnetic and Hydrogenation Properties of $RNiAl_2$ Ternary Compounds, *Lanthanide Actinide Res.*, 1986, **1**, p 153–161.
31. H. Oesterreicher, Structural and Magnetic Studies on Rare-Earth Compounds RNiAl and RCuAl, *J. Less-Comm. Met.*, 1973, **30**, p 225–236.
32. A.E. Dwight, M.H. Mueller, R.A. Conner, J.W. Downey, and H. Knott, Ternary Compounds with the Fe_2P-Type Structure, *Transactions of the Metallurgical Society of AIME*, 1968, **242**, p 2075–2080.
33. V.A. Yartys, and V.V. Parlenko, Investigation of the Interaction of Hydrogen with the Intermetallic Compounds $R_3Ni_6Al_2$ (R= Y, Sm, Gd, Dy, Ho, Er) with the Structure Type Ca_3Ag_8, *Koord. Khim.*, 1992, **18**, p 424–427.
34. N. Biliškov, G.I. Miletić, A. Drašner, and K. Prezelj, Structural and Hydrogen Sorption Properties of $SmNi_{5-x}Al_x$ System—An Experimental and Theoretical Study, *Int. J. Hydrogen Energy*, 2015, **40**, p 8548–8561.
35. W. Kraus, and G. Nolze, POWDER CELL—A Program for the Representation and Manipulation of Crystal Structures and Calculation of the Resulting x-Ray Powder Patterns, *J. Appl. Crystallogr.*, 1996, **29**, p 301–303.
36. D. Schwarzenbach, *LATCON: Refine Lattice Parameters*. University of Lausanne, Lausanne, Switzerland, 1966.
37. J. Bobet, S. Pechev, B. Chevalier, and B. Darriet, Structural and Hydrogen Sorption Studies of $NdNi_{5-x}Al_x$ and $GdNi_{5-x}Al_x$, *J. Alloys Compd.*, 1998, **267**, p 36–41.